Kinetic analysis methods applied to single motor protein trajectories

A L Nord[1], A F Pols[2], M Depken*[2], and F Pedaci*[1]

[1]CBS, Univ Montpellier, CNRS, INSERM, Montpellier, France
[2]Kavli Institute of NanoScience and Department of BioNanoScience, Delft University of Technology, Delft, 2629HZ, The Netherlands
*email: s.m.depken@tudelft.nl, francesco.pedaci@cbs.cnrs.fr

Molecular motors convert chemical or electrical energy into mechanical displacement, either linear or rotary. Under ideal circumstances, single-molecule measurements can spatially and temporally resolve individual steps of the motor, revealing important properties of the underlying mechanochemical process. Unfortunately, steps are often hard to resolve, as they are masked by thermal noise. In such cases, details of the mechanochemistry can nonetheless be recovered by analyzing the fluctuations in the recorded traces. Here, we expand upon existing statistical analysis methods, providing two new avenues to extract the motor step size, the effective number of rate-limiting chemical states per translocation step, and the compliance of the link between the motor position and the probe particle. We first demonstrate the power and limitations of these methods using simulated molecular motor trajectories, and we then apply these methods to experimental data of kinesin, the bacterial flagellar motor, and F_1-ATPase.

1 Intro

Molecular motors convert chemical and electrical energy into mechanical work in the form of linear or rotary motion. This process can be seen as a stochastic sequence of chemical and conformational changes driven by chemical-energy consumption and influenced by thermal forces. While bulk measurements are able to report on the average of the stochastic motion, they fail to capture the information contained in the single-molecule fluctuations. However, advances in single molecule techniques, which provide the opportunity to measure the movement of single motor proteins *in vivo* and *in vitro*, have proven remarkably valuable in the study of molecular motors. Given adequate spatio-temporal resolution, the mechanochemical reaction schemes of motor proteins can be resolved, providing details of the underlying microscopic mechanism [1]. Single

molecule experiments have enabled the direct resolution of individual steps in many molecular motors, revealing details of the mechanochemical cycle for kinesin [2,3], myosin [4–7], dynein [8,9], F_1-ATPase [10,11], the viral packaging motor $\phi 29$ [12,13], and the bacterial flageller motor [14]. Such measurements yield information about the fundamental mechanical step size, the number of chemical processes per mechanical step, the transition rate between states, and the number of fuel molecules consumed per mechanochemical cycle.

Despite great experimental advances, the signal-to-noise ratio of single motor trajectories is often insufficient to resolve individual motor steps. Under these conditions, analysis of the stochastic fluctuations can provide information not deducible from average quantities. For example, in the time domain, measurements of the variance in displacement have yielded the number of rate-limiting processes and the number of ATP molecules consumed per mechanochemical cycle of kinesin [15–17]. In the frequency domain, the underlying stochastic signal and the noise often have separable power spectra, and can thus be identified and characterized in Fourier space, yielding the number of rate-limiting steps in the enzymatic cycle [18]. Such analysis has further yielded the step size of UvrD helicase [19] and DNA translocase FtsK [20], and the relaxation step of DNA supercoiling type II topoisomerase [18].

In this study, we extend previous work in order to provide analytical solutions to i) the steady-state variance of a reporter-particle displacements over fixed time intervals and ii) the power spectrum of the speed of the reporter particle. Under certain conditions, these methods, one of which operates in the time domain and the other in the frequency domain, are capable of recovering the mechanical step size of the motor, the number of chemical processes per step, and the stiffness of the linker between the motor protein and probe, even under conditions where the individual steps are not spatially and temporally resolved. We perform simulations to compare the performance of these methods, and we demonstrate their utility in extracting additional information from previously published experimental data of three molecular motors.

2 Theoretical analysis of single motor trajectories

In order to extract additional information from the stochastic fluctuations of a reporter particle, we need to model the effects of the underlying mechanochemical cycle on its motion. In a classical approach to macromolecular dynamics [15], which shares several aspects with the treatment of shot noise in physical systems [21, 22], the displacement $x_{\mathrm{b}}(t)$ of the observable reporter object, often a microscopic bead, tethered to the molecular motor is modeled by

$$x_{\mathrm{b}}(t) = aN(t) + \eta(t). \qquad (1)$$

Here a is the size of the mechanical step of the motor along its track, $N(t)$ is the total number of mechanical steps in time t, and η is the thermal noise characterized by $\langle \eta \rangle = 0$ and $\langle \eta^2 \rangle = k_{\mathrm{B}}T/k_l$, where k_l is the total stiffness of the construct. Implicit in this description is further that the response of the system is faster than any other relevant timescale of the system, including the motor stepping rate. This condition might not always be clearly satisfied *a priori*, and we relax this condition by instead modeling the bead motion as governed by Stoke's drag (drag coefficient

2

γ)

$$\gamma \frac{dx_{\mathrm{b}}}{dt}(t) = k_l(aN(t) - x_{\mathrm{b}}(t)) + \xi(t). \tag{2}$$

where the random force $\xi(t)$ satisfies [23]

$$\langle \xi(t) \rangle = 0, \quad \langle \xi(t)\xi(t') \rangle = 2\gamma k_B T \delta(t - t'), \tag{3}$$

and δ is the Dirac-delta function.

2.1   Time-domain analysis of reporter-particle position fluctuations

In the case that the motor is a Poisson stepper, and the reporter particle instantaneously responds to motor displacements (i.e. when Equation (1) holds), both the average and variance of the reporter-particle displacement increases linearly with time in the steady state [15]

$$\langle \Delta x_{\mathrm{b}}(t) \rangle = vt, \quad var(\Delta x_{\mathrm{b}}(t)) = \frac{2k_{\mathrm{B}}T}{k_l} + avt, \quad \Delta x_{\mathrm{b}}(t) = x_{\mathrm{b}}(t_0 + t) - x_{\mathrm{b}}(t_0). \tag{4}$$

The utility of this approach comes from the fact that Eq (4) can be used to estimate the step size a and construct stiffness k_l by analyzing the average and variance of the experimentally accessible reporter-particle displacements. More precisely, Eq (4) shows that

$$a = \left. \frac{\partial var(\Delta x_{\mathrm{b}}(t))}{\partial t} \middle/ v \right|_{t>0}, \quad k_l = \left. \frac{2k_B T}{var(x_{\mathrm{b}}(t))} \right|_{t=0}. \tag{5}$$

More generally, if the step size is known, the randomness parameter

$$r = \left. \frac{\partial var(\Delta x_{\mathrm{b}}(t))}{\partial t} \middle/ av \right|_{t>0} \tag{6}$$

has been introduced [15] to quantify how much the process deviates from Poisson statistics ($r = 1$). In the simple case where only every m:th chemical step gives rise to translocation, it can be shown that $r = 1/m$, and if we know the step size we can estimate how many effective chemical steps there is in one translocation cycle [15].

As we aim to also capture the relaxation dynamics of the system, we extend the above analysis by considering the variance and average displacement of a reporter particle that moves according to Eq. (2). Assuming that the molecular motor is a Poisson stepper, wherein each mechanical step of the motor is a consequence of a single rate-limiting biochemical process we find that the variance of the bead position can be expressed as (see derivation in the SI)

$$var(x_{\mathrm{b}}(t)) = \frac{2k_{\mathrm{B}}T + av\gamma}{k_l}(1 - e^{-2k_l t/\gamma}) + avt. \tag{7}$$

It is worth noting that this expression of the variance expands the classical result described above by Eq (4), including the filtering effect of the elastic linkage, which imposes a characteristic

3

relaxation time $t_c = \gamma/k_l$. In the limit of $t_c \to 0$, Eq (4) is retrieved from Eq (7). Therefore, by measuring the bead position $x_\mathrm{b}(t)$, its variance $var(x_\mathrm{b}(t))$ can be calculated and fit with Eq (7) to obtain the relaxation time (or equivalently the drag), as well as the step size a and the construct stiffness k_l. Fig S1F-I demonstrate the behavior of Eq (7) as a function of motor step size, motor speed, stiffness of the linker, and bead size. It is interesting to note that if the average energy dissipated by moving the bead a distance equal to the motor step ($av\gamma$) is not negligible compared to twice the thermal energy ($2k_\mathrm{B}T$), then we will underestimate the construct stiffness if we assume the dynamics to be governed by Eq. (1).

2.2 Frequency-domain analysis of reporter-particle velocity fluctuations

Instead of analyzing the motor position in the time domain, we now approach the molecular system by analyzing the speed of the motor in the frequency domain. In the time domain, characteristic behaviors on different timescales are convoluted, and often hard to disentangle. In the frequency domain such time-separated behaviors are often readily disentangled as they affect different frequency ranges. This is true, for instance, for low signal-to-noise measurements where the signal and noise, due to their statistics, can by separated and identified in the Fourier domain [18]. Below we show that an analysis of the speed of the motor in the frequency domain provides the interesting ability of simultaneously quantifying step size, construct stiffness, and relaxation time of the molecular system. In the frequency domain we further manage to extend our considerations to the situation where only every m:th chemical cycle results in translocation, allowing us to estimate also the effective number of rate-limiting chemical steps for each translocation step.

Taking the Fourier transform of Eq (2) (derived in SI), the power spectral density (PSD) of the speed of the bead velocity ($v_\mathrm{b} = dx_\mathrm{b}/dt$) as a function of frequency f (measured in Hz) can be written as

$$S_{v_\mathrm{b}}(f) = \frac{1}{(2\pi f t_c)^2 + 1} S_{v_\mathrm{m}}(f) + \frac{1}{\gamma^2} \frac{(2\pi f t_c)^2}{(2\pi f t_c)^2 + 1} S_\xi(f), \tag{8}$$

where $t_c = \gamma/k_l$ is the characteristic relaxation time of the construct. The two components S_{v_m} and S_ξ are the PSD of the speed of the motor v_m, and the PSD of the thermal forces ξ acting on the bead, respectively. By direct analogy to shot noise in electronic circuits (see SI), the PSD of the motor's velocity can be written as

$$S_{v_\mathrm{m}} = a\langle v_\mathrm{m}\rangle = av, \tag{9}$$

in the steady state. We note here that S_{v_m} is independent of frequency. The PSD of the thermal forces acting on the bead can be computed by applying the Wiener-Khinchin theorem [24] to Eqs (3), giving

$$S_\xi = \int_{-\infty}^{\infty} \langle \xi(t)\xi(t+\tau)\rangle e^{-i\omega t} = 2\gamma k_\mathrm{B}T. \tag{10}$$

Note that the above term is independent of frequency as well, i.e. the thermal forces acting on the bead produce white noise. Finally, combining Eqs (8), (9), and (10), the explicit analytical

4

expression for the PSD of the speed of a bead v_b elastically tethered to a Poissonian stepping motor can be written as

$$S_{v_{\mathrm{b}}}(f) = \frac{av}{(2\pi f t_c)^2 + 1} + \frac{2k_{\mathrm{B}}T}{\gamma} \frac{(2\pi f t_c)^2}{(2\pi f t_c)^2 + 1}. \tag{11}$$

This result can be generalized to the situation where only every m:th chemical step gives rise to translocation of the motor. Letting τ be the average time between translocation events, we find that the PSD of the motor speed, gains an extra factor α (derived in the SI), $S_{v_{\mathrm{m}}} = av\alpha(f)$, with

$$\alpha(f) = 1 + \frac{1}{(1 - 2\pi i f \tau/m)^m - 1} + \frac{1}{(1 + 2\pi i f \tau/m)^m - 1}. \tag{12}$$

Therefore in this more general case, the overall PSD of the speed of the bead becomes

$$S_{v_b}(f) = \frac{av\alpha(f)}{(2\pi f t_c)^2 + 1} + \frac{2k_{\mathrm{B}}T}{\gamma} \frac{(2\pi f t_c)^2}{(2\pi f t_c)^2 + 1}. \tag{13}$$

We note that in the case of a pure Poisson stepper $(m = 1)$, $\alpha = 1$ and Eq (13) reduces to Eq (11). Fig S1A-E demonstrate the behavior of Eq (13) as a function of motor step size, motor speed, construct stiffness, probe size, and the number of rate-limiting chemical transitions.

3   Materials and methods

3.1   Motor simulations

Kinetic Monte Carlo (KMC) methods, performed in Python, were used to model a Poisson stepper and obtain the motor trace $x_m(t)$, which was then used to obtain the bead trace $x_{\mathrm{b}}(t)$ by integrating Eq (2). The input parameters were the mechanical step size a, the number m of (equally rate-limiting) chemical processes per mechanochemical step, the rate k for each of the m transitions, the stiffness k_l of the elastic linkage, and the radius r_b of the attached particle. The integration time was set to $t_c/15$, where $t_c = \gamma/k_l$ was the bead relaxation time.

3.2   Time domain analysis of position fluctuations

The displacement of the bead was calculated over integer numbers of points for each trace, and the variance of the displacement was plotted as a function of time. A weighted least square fit of Eq (7) was computed for a time interval of zero to $1/100$ the trace duration, yielding the motor step size, a, and the linker stiffness, k_l. Errors were calculated by performing 50 simulations with input parameters which matched the fit parameters of each of the experimental motors, then calculating the mean error of a and k_l over all the simulations.

5

3.3 Frequency domain analysis of velocity fluctuations

The normalized, one-sided, log-binned, power spectral density (PSD) of the bead's speed was calculated for each trace. A least squares fit of Eq (13) to the PSD was performed to optimize the free parameters of motor step size, a, the stiffness of the system, k_l, the number of rate-limiting steps, m, and for the experimental data, the drag of the system, γ. The average velocity of the motor, $\langle v_{\mathrm{m}} \rangle$, was calculated as the total angular distance traveled divided by the total time of the trace. Errors were calculated by performing 50 simulations with input parameters which matched the fit parameters of each of the experimental motors, then calculating the mean error of a and k_l over all the simulations.

4 Results

4.1 Simulated molecular motor rotation

Using simulations of a linear Poisson stepping motor (see Materials and Methods), we have tested the performance of each analysis method described above over a biologically relevant range of step sizes and linkage compliances. Fig 1 shows an example of such simulations and the analysis via the two methods. We performed fits of the simulated data, and the results of this analysis are shown in Fig 2. These simulations model a large load (1 μm bead) attached to the motor; see SI, Fig S3, for similar simulations of a small load (30 nm bead) attached to the motor.

We emphasize that the results shown in Fig 2 and Fig S3 are highly dependent upon the characteristics of both the motor and the experimental measurement. For example, with the frequency domain analysis of velocity fluctuations, recovery of the step size improves with longer measurements (yielding lower frequencies in the power spectrum), while recovery of the stiffness improves with higher acquisition rates (yielding higher frequencies in the power spectrum). Thus, simulations are a useful tool either to optimize such parameters prior to experiments or to explore under what circumstances these methods are applicable. In the following, we challenge the analysis methods developed above to extract the mechanical features of three molecular motors, whose parameters have been already independently assessed.

4.2 Kinesin

Kinesin is a cytoskeletal molecular motor which hydrolyzes ATP in order to move unidirectionally along microtubules, driving active cellular processes such as the transportation of molecular cargo. Moving with a 'hand-over-hand' technique, the heads of Kinesin-1 take 16 nm steps along the microtubule [25, 26]. Kinesin-1 is a model system for the study of molecular motors and development of single-molecule techniques [15, 27].

Fig 3A shows the translation of *Drosophila* kinesin-1 along an immobilized microtubule at saturating ATP concentration, tracked at 1 kHz via a gold nanoparticle (30 nm diameter) attached to one N-terminal head of the dimeric motor (data from Mickolajczyk et al [28]). Fig 3B shows the power spectrum (points) and fit (line) of the speed of the motor. The fit of the power spectrum

6

177 yields a step size a=16 $\pm$ 4 nm, where m=4 states are present per two mechanochemical cycles
178 (as only one head is labeled), with a total stiffness k_l=0.06 $\pm$ 0.05 pN/nm. The retrieved
179 step is in agreement with the 16.4 nm step resolved in the time domain, and expected by the
180 displacement of a single head along the microtubule. At saturating [ATP], the total duration
181 of the mechanochemical cycle is evenly split between 1 head-bound (HB) and 2HB states [28],
182 each of which contain one rate-limiting step [3, 29]. Thus, for saturating [ATP] assays in which
183 a single head is labeled, one expects four rate-limiting processes per step, validating the value of
184 $m = 4$ found here. Time domain analysis of position fluctuations (Fig S1B) yields a step size
185 of 4.4 $\pm$ 0.9 nm; given four rate-limiting processes per step, this measurement is expected to
186 be underestimated by a factor of 4, and is thus in agreement with the power spectral analysis.
187 Finally, the total stiffness found from the fit in Fig 3B likely reflects a weighted average value of
188 the stiffness of the system in the 1HB and 2HB states.

189   4.3   Bacterial flagellar motor

190 The bacterial flagellar motor (BFM) is the rotary molecular motor which rotates a flagellar filament
191 of many species of motile bacteria, enabling swimming, swarming, and chemotaxis. Resolution
192 of the fundamental step of the BFM has long proven difficult due to the rapid speed of motor
193 rotation (up to 300 Hz in *E. coli* [30]), and the soft torsional compliance of the hook, which
194 connects the rotor to the filament [31]. Using single molecule measurements of a particle attached
195 to the filament of an immobilized bacterial cell, Sowa et al successfully resolved individual steps
196 of the BFM under severely deenergized conditions [14].
197   Fig 3C shows the rotation of a polystyrene bead (227 nm diameter) attached to a truncated
198 flagellar filament of a single BFM on a surface-immobilized *E. coli* cell (data from Sowa et al [14]).
199 The speed of the motor was slowed via low expression of stator proteins and photodamage from
200 the illumination source. Fig 3D shows the power spectrum of the speed of this trace (points) and
201 theoretical best fit (line). The fit of the power spectrum yields a step size of 11.7 $\pm$ 0.5 degrees,
202 equivalent to 31 $\pm$ 1 steps per revolution. This result is compatible with the results obtained by
203 Sowa et al (13.8 degrees, 26 steps per revolution) [14], and also with the 26- or 34-fold symmetric
204 ring of FliG molecules, the 'track' upon which the stators generate torque [32, 33]. Time domain
205 analysis of position fluctuations (Fig S1C-D) yields a slightly larger step size, 38 $\pm$ 1 degrees,
206 potentially affected by speed fluctuations during the trace (see SI). The fit of the power spectrum
207 yields a stiffness of 1400 $\pm$ 400 pN nm/rad. Previous measurements have determined that the
208 torsional compliance of the BFM is dominated by the compliance of the hook (instead of the
209 filament) [31], and estimates of the torsional compliance of the hook span an order of magnitude,
210 from $100 - 1300$ pN nm rad^{-1} [31, 34, 35]. Our result is consistent with the upper range of these
211 measurements.

212   4.4 F_1 ATPase

213 F_1F_O ATP synthase is the rotary molecular motor responsible for the synthesis of ATP in bacteria
214 and eukaryotes. The enzyme is in fact comprised of two separable coaxial molecular motors, F_O

215 and F_1. On its own, F_1 behaves as an ATP-hydrolyzing enzyme, the mechanochemical cycle of
216 which has been well established by extensive single molecules studies [36]. Briefly, the rotation
217 of F_1 is comprised of six steps [11], of alternating size $80°$ and $40°$. F_1 consumes three ATP
218 molecules per rotation (one for each of its catalytic sites); each ATP-binding dwell (three per
219 rotation) shows single-exponential kinetics, and each catalytic dwell (also three per rotation)
220 shows at least double-exponential kinetics, due to ATP hydrolysis and phosphate release [37–39].
221   Fig 3E shows the rotation of a 60 nm gold bead attached the the γ subunit of a single surface-
222 immobilized yeast F_1-ATPase (data from Steel et al [40]). The ATP concentration in the flow cell
223 was changed from low to high (5 μM to 3 mM) during the recording, evidenced by the change in
224 rotation speed. Fig 3F shows the power spectra (points) and fit (line) of the highlighted sections
225 of Fig 3E for low [ATP] and high [ATP] (blue and green, respectively). The fit of the low [ATP]
226 spectrum yields 3.0 ± 0.4 steps per revolution, where $m = 1$ states are present, consistent with
227 previous results which show 3 steps per revolution at low [ATP] [10], and show that this step
228 of the mechanochemical cycle is limited by a single reaction, ATP-binding [11]. Time domain
229 analysis of position fluctuations (Fig S1F-G) yields 2.7 ± 0.4 steps per revolution. The fit of
230 Fig 3F for high [ATP] yields 3.8 ± 0.5 steps per revolution, where $m = 3$ states are present per
231 mechanochemical cycle, yielding 11.4 ± 1.5 processes per revolution. Our model assumes that
232 each step of the motor consists of the same number of Poisson processes, an assumption that
233 doesn't hold for F_1 at non-limiting [ATP]. Nonetheless, the fit is consistent with 3-4 rate-limiting
234 processes per catalytic site per revolution [41]. Time domain analysis of position fluctuations
235 (Fig S1F-G) yields 7.2 ± 4 steps per revolution, also consistent with the number of rate-limiting
236 mechanochemical processes. Interestingly, the fits of Fig 3F at low and high [ATP] yield a stiffness
237 of 21 ± 4 and 23 ± 3 pN nm/rad respectively, consistent with a previous measurement of 30 pN
238 nm/rad and 66 pN nm/rad at the ATP-waiting and catalytic dwells, respectively [42].

239 5   Discussion

240 We have presented two new analytical solutions which are capable of extracting key features of the
241 mechanochemical cycle of a molecular motor from single experimentally measured trajectories.
242 We have used simulations to measure the performance of these methods under two quite different
243 experimental conditions, and we have applied these methods to previously published data of three
244 molecular motors.
245   Our simulations show that, with respect to recovering the step size, the stiffer the linker
246 the better. This is apparent in both of the analysis methods, and most pronounced in the time
247 domain analysis of position fluctuations, wherein a compliant linker lengthens the relaxation time
248 of the system, introducing a correlation between dwell times. As stiffness increases, the methods
249 perform similarly. Fig S3 compares these methods to a third method in which the distribution
250 of the dwell time of the reporter particle over a defined window size allows the determination of
251 the number of sequential steps within the window [43–46]. For our simulations, the two methods
252 developed here recover the step size with better accuracy and lower error than the dwell time
253 analysis method (see SI for discussion). We note that, while a stiffer linker improves recovery of

254 step size, it may also increase the probability of interactions between the reporter-particle and
255 motor which may disturb motor function.

256   Figs 2A and S3A show the recovery of the step size as a function of the ratio between the
257 standard deviation of the noise and the step size. Crucially, these plots show good recovery of
258 the step size up to and far beyond the limits of traditional step detection algorithms [47, 48],
259 emphasizing the utility of these methods in situations where steps are not able to be resolved.

260   Simulations show that both the time domain analysis of position fluctuations and the frequency
261 domain analysis of velocity fluctuations are able to recover the stiffness of the linker between the
262 reporter particle and motor, showing little dependence on the step size. At both large and small
263 loads, the two methods produce similar accuracy and error, at least for a compliant linker. As
264 the stiffness increases, the accuracy of the time domain analysis of position fluctuations drops
265 dramatically. The frequency domain analysis of velocity fluctuations performs better at higher
266 stiffness, though simulations of a small load (where the corner frequency of the power spectrum
267 shifts towards higher frequencies) show that recovery of the stiffness is affected by systematic
268 errors associated with the discrete power spectra, such as aliasing and spectral leakage [49].

269   These two methods obviate the need for step-detection algorithms, which are often sensitive to
270 user-set parameters [47, 50], and which prove of little use when the noise becomes of the order or
271 larger than the step size. Furthermore, these methods are complementary, though we emphasize
272 that simulations are useful to determine the accuracy and error of each method for a particular
273 experiment. While both methods are based on the assumption of a Poisson stepper, where the
274 time between two successive steps is exponentially distributed and the step size is constant,
275 the frequency domain analysis of velocity fluctuations has the ability to further decipher the
276 number of chemical processes per mechanical step in situations where the time between steps is a
277 convolution of multiple exponentials. Both methods will be affected by off-pathway states, such
278 as pauses, which are common amongst many molecular motors, though we note that this affects
279 only the recovery of the step size, not the linker stiffness. Thus, the statistical analysis methods
280 presented here provide a powerful mechanism of extracting kinetic features which are otherwise
281 often invisible within single-molecule data.

Acknowledgments

Competing financial interests

291 The authors declare no conflict of interest.

²⁹² **Materials & Correspondence**

²⁹³ To whom correspondence should be addressed: s.m.depken@tudelft.nl or francesco.pedaci@cbs.cnrs.fr

References

[1] Bustamante, C., Chemla, Y. R., Forde, N. R. & Izhaky, D. Mechanical processes in biochemistry. *Annual Review of Biochemistry* **73**, 705–748 (2004).

[2] Svoboda, K., Schmidt, C. F., Schnapp, B. J. & Block, S. M. Direct observation of kinesin stepping by optical trapping interferometry. *Nature* **365**, 721–7 (1993).

[3] Visscher, K., Schnitzer, M. & Block, S. Single kinesin molecules studied with a molecular force clamp. *Nature* **400**, 184–189 (1999).

[4] Veigel, C. *et al.* The motor protein myosin-I produces its working stroke in two steps. *Nature* **398**, 530–533 (1999).

[5] Finer, J. T., Simmons, R. M. & Spudich, J. A. Single myosin molecule mechanics: piconewton forces and nanometre steps. *Nature* **368**, 113–9 (1994).

[6] Rock, R. S. *et al.* Myosin VI is a processive motor with a large step size. *Proceedings of the National Academy of Sciences of the United States of America* **98**, 13655–13659 (2001).

[7] Mehta, A. D. *et al.* Myosin-V is a processive actin-based motor. *Nature* **400**, 590–3 (1999).

[8] Hirakawa, E., Higuchi, H. & Toyoshima, Y. Y. Processive movement of single 22s dynein molecules occurs only at low ATP concentrations. *Proceedings of the National Academy of Sciences of the United States of America* **97**, 2533–2537 (2000).

[9] Mallik, R., Carter, B., Lex, S., King, S. & Gross, S. Cytoplasmic dynein functions as a gear in response to load. *Nature* **427**, 649–652 (2004).

[10] Yasuda, R., Noji, H., Kinosita, K. J. & Yoshida, M. F_1-ATPase is a highly efficient molecular motor that rotates with discrete 120 degree steps. *Cell* **93**, 1117–24 (1998).

[11] Yasuda, R., Noji, H., Yoshida, M., Kinosita, K. & Itoh, H. Resolution of distinct rotational substeps by submillisecond kinetic analysis of f1-atpase. *Nature* **410** (2001).

[12] Yu, J., Moffitt, J., Hetherington, C. L., Bustamante, C. & Oster, G. Mechanochemistry of a viral DNA packaging motor. *Journal of molecular biology* **400**, 186–203 (2010).

[13] Chemla, Y. R. *et al.* Mechanism of force generation of a viral DNA packaging motor. *Cell* **122**, 683–692 (2005).

[14] Sowa, Y. *et al.* Direct observation of steps in rotation of the bacterial flagellar motor. *Nature* **437**, 916–9 (2005).

10

[15] Svoboda, K., Mitra, P. P. & Block, S. M. Fluctuation analysis of motor protein movement and single enzyme kinetics. *Proceedings of the National Academy of Sciences of the United States of America* **91**, 11782–6 (1994).

[16] Svoboda, K. & Block, S. Biological applications of optical forces. *Annual review of biophysics and biomolecular structure* **23**, 247–285 (1994).

[17] Schnitzer, M. J. & Block, S. M. Kinesin hydrolyses one ATP per 8-nm step. *Nature* **388**, 386–90 (1997).

[18] Charvin, G., Bensimon, D. & Croquette, V. On the relation between noise spectra and the distribution of time between steps for single molecular motors. *Single Molecules* **3**, 43–48 (2002).

[19] Dessinges, M., Lionnet, T., Xi, X., Bensimon, D. & Croquette, V. Single-molecule assay reveals strand switching and enhanced processivity of UvrD. *Proceedings of the National Academy of Sciences of the United States of America* **101**, 6439–44 (2004).

[20] Saleh, O. A., Pérals, C., Barre, F.-X. & Allemand, J.-F. Fast, DNA-sequence independent translocation by FtsK in a single-molecule experiment. *The EMBO journal* **23**, 2430–2439 (2004).

[21] Schottky, W. About spontaneous power fluctuations in different electricity conductors. *Annalen der Physik* **362**, 541–567 (1918).

[22] Neuman, K. C. *et al.* Statistical determination of the step size of molecular motors. *Journal of Physics: Condensed Matter* **17** (2005).

[23] Reif, F. *Fundamentals of Statistical and Thermal Physics* (McGraw-Hill, New York, 2009).

[24] Chatfield, C. *The Analysis of Time Series: An Introduction*, 94–95 (Chapman and Hall/CRC, 1989), 4th edn.

[25] Asbury, C. Kinesin: world's tiniest biped. *Current opinion in cell biology* **17** (2005).

[26] Yildiz, A., Tomishige, M., Vale, R. D. & Selvin, P. R. Kinesin walks hand-over-hand. *Science* **303**, 676–8 (2004).

[27] Mickolajczyk, K. J. & Hancock, W. O. Kinesin processivity is determined by a kinetic race from a vulnerable one-head-bound state. *Biophysical journal* **112**, 2615–2623 (2017).

[28] Mickolajczyk, K. J. *et al.* Kinetics of nucleotide-dependent structural transitions in the kinesin-1 hydrolysis cycle. *Proceedings of the National Academy of Sciences of the United States of America* **112**, E7186–E7193 (2015).

[29] Hancock, W. O. The kinesin-1 chemomechanical cycle: stepping toward a consensus. *Biophysical journal* **110**, 1216–1225 (2016).

11

[30] Yuan, J. & Berg, H. C. Resurrection of the flagellar rotary motor near zero load. *Proceedings of the National Academy of Sciences of the United States of America* **105**, 1182–5 (2008).

[31] Block, S. M., Blair, D. F. & Berg, H. C. Compliance of bacterial polyhooks measured with optical tweezers. *Cytometry* **12**, 492–6 (1991).

[32] Lee, L. K., Ginsburg, M. A., Crovace, C., Donohoe, M. & Stock, D. Structure of the torque ring of the flagellar motor and the molecular basis for rotational switching. *Nature* **466**, 996–1000 (2010).

[33] Stock, D., Namba, K. & Lee, L. K. Nanorotors and self-assembling macromolecular machines: the torque ring of the bacterial flagellar motor. *Current opinion in biotechnology* **23**, 545–554 (2012).

[34] Block, S. M., Blair, D. F. & Berg, H. C. Compliance of bacterial flagella measured with optical tweezers. *Nature* **338**, 514–8 (1989).

[35] Brown, M. T. *et al.* Flagellar hook flexibility is essential for bundle formation in swimming Escherichia coli cells. *Journal of Bacteriology.* **194**, 3495–3501 (2012).

[36] Watanabe, R. & Noji, H. Chemomechanical coupling mechanism of F_1-ATPase: catalysis and torque generation. *FEBS letters* **587**, 1030–1035 (2013).

[37] Adachi, K. *et al.* Coupling of rotation and catalysis in F_1-ATPase revealed by single-molecule imaging and manipulation. *Cell* **130**, 309–21 (2007).

[38] Shimabukuro, K. *et al.* Catalysis and rotation of F_1 motor: cleavage of ATP at the catalytic site occurs in 1 ms before 40 degree substep rotation. *Proceedings of the National Academy of Sciences of the United States of America* **100**, 14731–6 (2003).

[39] Watanabe, R., Iino, R. & Noji, H. Phosphate release in F_1-ATPase catalytic cycle follows ADP release. *Nature Chemical Biology* **6**, 814–20 (2010).

[40] Steel, B. C. *et al.* Comparison between single-molecule and x-ray crystallography data on yeast F_1-ATPase. *Scientific Reports* **5** (2015).

[41] Okuno, D., Iino, R. & Noji, H. Rotation and structure of F_oF_1-ATPase. *The Journal of Biochemistry* **149**, 655–664 (2011).

[42] Sielaff, H. *et al.* Domain compliance and elastic power transmission in rotary F_oF_1-ATPase. *Proceedings of the National Academy of Sciences of the United States of America* **105** (2008).

[43] Lucius, A. L., Maluf, N. K., Fischer, C. J. & Lohman, T. M. General methods for analysis of sequential "n-step" kinetic mechanisms: Application to single turnover kinetics of helicase-catalyzed DNA unwinding. *Biophysical journal* **85**, 2224–2239 (2003).

[44] Xie, S. Single-molecule approach to enzymology. *Single Molecules* **2**, 229–236 (2001).

[45] Zhou, Y. & Zhuang, X. Kinetic analysis of sequential multistep reactions. *The Journal of Physical Chemistry B* **111**, 13600–13610 (2007).

[46] Floyd, D. L., Harrison, S. C. & Van Oijen, A. M. Analysis of kinetic intermediates in single-particle dwell-time distributions. *Biophysical journal* **99**, 360–366 (2010).

[47] Carter, B. C., Vershinin, M. & Gross, S. P. A comparison of step-detection methods: How well can you do? *Biophysical journal* **94**, 306–319 (2008).

[48] Chen, Y., Deffenbaugh, N. C., Anderson, C. T. & Hancock, W. O. Molecular counting by photobleaching in protein complexes with many subunits: best practices and application to the cellulose synthesis complex. *Molecular Biology of the Cell* **25**, 3630–3642 (2014).

[49] Mack, C. A. Systematic errors in the measurement of power spectral density. *Journal of Micro/Nanolithography MEMS and MOEMS* **12** (2013).

[50] Kerssemakers, J. W. J. *et al.* Assembly dynamics of microtubules at molecular resolution. *Nature* **442**, 709–712 (2006).
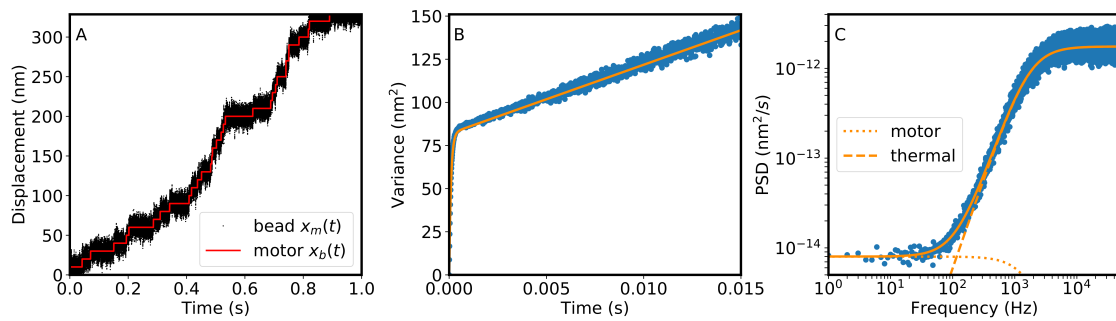
Figure 1: An example of the simulations used to test the three analysis methods. A) The simulated displacement versus time of a motor (red) and the attached bead (black). The first 1 s of a 60 s simulation is shown here; the full simulation was used for B-D. Simulation parameters: $r_b = 500$ nm, $\langle v_{\mathrm{m}} \rangle = 400$ nm/s, $a = 10$ nm, $k_l = 1 \cdot 10^{-5}$ N/m. B) The variance of the reporter-particle displacement $var(\Delta x_b(t))$ as a function of time for the simulated trace (blue points), and theory (Eq (7), orange line). C) The PSD of the speed of the bead (blue points) and theory (Eq (11), solid orange line). The dotted and dashed line show the components of the PSD attributed to the movement of the motor and the thermal noise on the bead, respectively. This PSD is an average of 60 PSDs taken on 1 s non-overlapping windows over the trace.
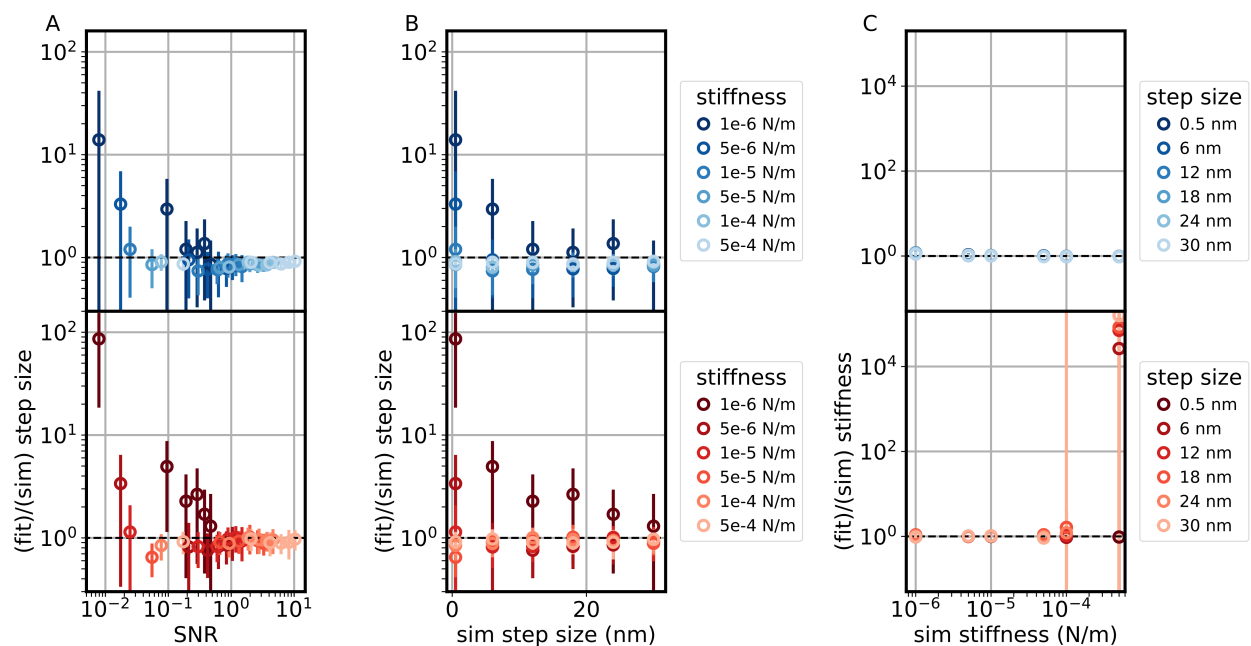

Figure 2: The performance of the frequency domain analysis of velocity fluctuations (blue) and time domain analysis of position fluctuations (red) analysis on simulated traces of a linear motor driving a 1 μm bead at 400 nm/s with step size and stiffness as labeled. A) Ratio of the extracted step size to the simulated step size as a function of the signal to noise ration (SNR), defined as the simulated step size divided by the standard deviation of the difference between the bead position and motor position. B) Ratio of the extracted step size to the simulated step size as a function of the simulated step size. C) Ratio of the fit stiffness to the simulated stiffness as a function of the simulated stiffness. The dashed black lines represent perfect recovery of the input parameters. Points and error bars represent mean and standard deviation over 30 simulations (2 s each) per point.
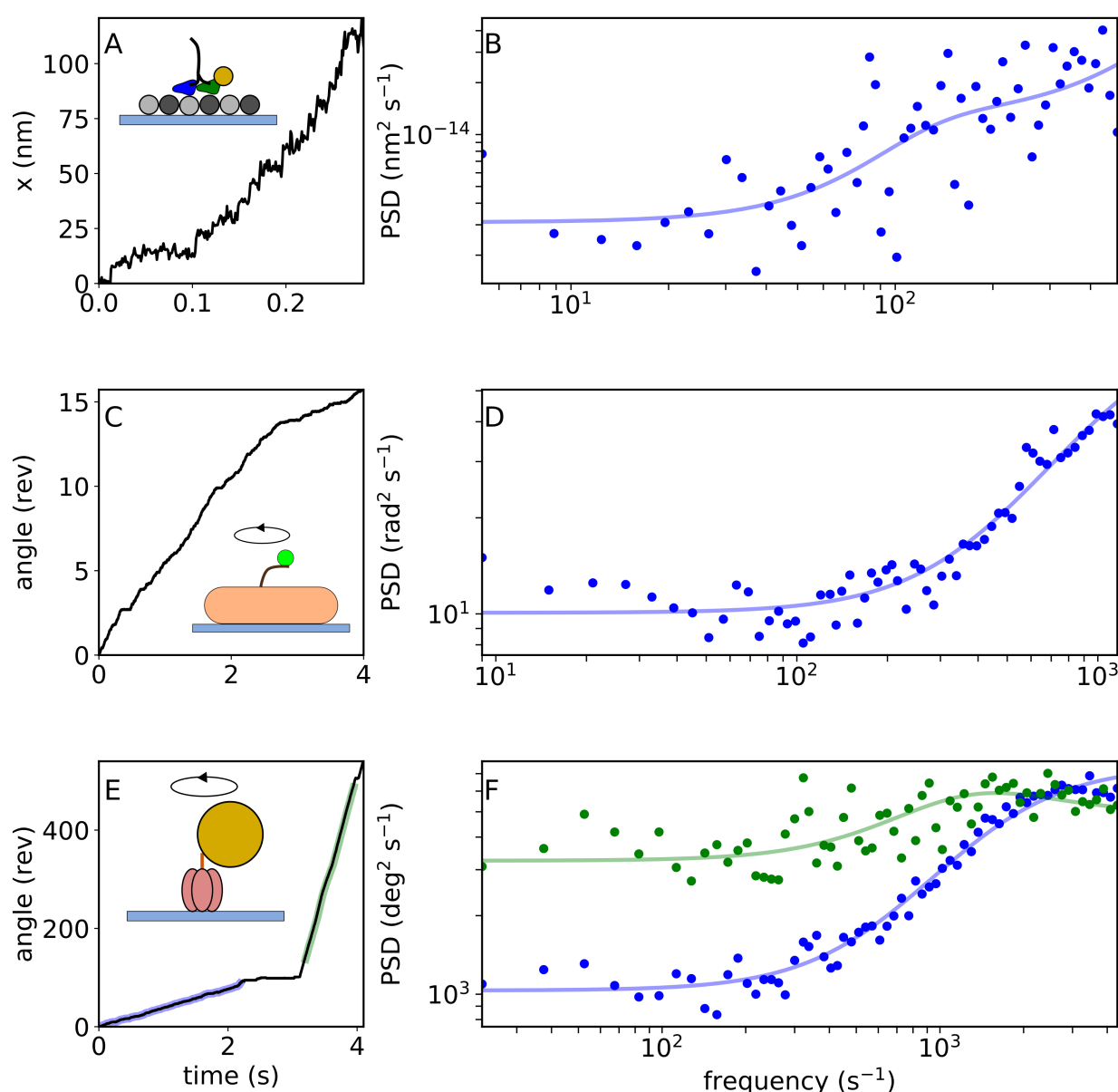
Figure 3: Experimental data of three molecular motors. A) Translation of *Drosophila* kinesin-1 along an immobilized microtubule, at saturating [ATP], tracked via a gold nanoparticle attached to one N-terminal head [27, 28]. Inset shows assay schematic. B) Points show the PSD of the speed of trace (A), and the line shows the best fit. (Fit parameters – $m = 4$; $a = 16.3$ nm; $k_l = 0.06$ pN /nm). C) Rotation of a bead attached to a truncated flagellar filament of a single BFM on a surface-immobilized *E. coli* cell [14]. Inset shows assay schematic. D) Points show the PSD of the speed of trace (C), and the line shows the best fit. (Fit parameters – $m = 1$; $a = 11.7°$; $k_l = 1443$ pN nm/rad). E) Rotation of a bead attached to the γ subunit of a single surface-immobilized yeast F_1-ATPase [40]. Inset shows assay schematic. F) Points show the PSD of the speed of highlighted segments of trace (E), and the line shows the best fit. (Fit parameters – low [ATP] (blue): $m = 1$; $a = 118°$; $k_l = 21$ pN nm/rad; high [ATP] (green): $m = 3$; $a = 95°$; $k_l = 23$ pN nm/rad).